

Charge-exchange reaction cross sections and the Gamow-Teller strength for double beta decay

K. Amos*

School of Physics, University of Melbourne, Victoria 3010, Australia

Amand Faessler[†] and V. Rodin[‡]

Institute of Theoretical Physics, University of Tuebingen, 72076 Tuebingen, Germany

(Dated: February 9, 2020)

Abstract

The proportionality between single charge-exchange reaction cross sections in the forward direction as found, for example from (p, n) and $(^3\text{He}, t)$ and from (n, p) and $(d, ^2\text{He})$ reactions, and the Gamow-Teller (GT) strength into the same final nuclear states has been studied and/or assumed often in the past. We demonstrate for medium-heavy nuclei undergoing double beta-decay, that the proportionality is a relative good assumption for reactions changing a neutron into a proton, e.g. (p, n) and $(^3\text{He}, t)$. In this channel, the main contribution to the GT strengths comes from the removal of a neutron from an occupied single-particle (SP) state and putting a proton into an unoccupied SP state having either the same state quantum numbers or those of the spin-orbit partner. In contrast to this, in the second leg of the double beta decay a single proton must be taken from an occupied SP state and a neutron placed in an unoccupied one. This second process often is Pauli forbidden in medium-heavy nuclei and only can be effected if the Fermi surface is smeared out. We show herein that one may not always assume a proportionality between the forward-angle cross sections of the charge-exchange reactions like (n, p) and $(d, ^2\text{He})$ and the GT strength in medium-heavy nuclei. The discrepancy in this channel originates e.g. from the radial dependence of the nucleon-nucleon (NN) interaction. Such a radial dependence is completely absent in the GT transition operator.

I. INTRODUCTION

In recent years, interest in the relation between charge-exchange reactions in the forward direction and the GT strength has increased due to the connection of the GT strength with the two-neutrino double beta decay [1, 2, 3, 4, 5]. The latter process may help to test the nuclear wave functions required in calculations of the matrix elements for the neutrinoless double beta decay. The neutrinoless double beta-decay transition probability is important since it, in con-

junction with measured data and assuming that the light neutrino exchange is the leading contribution, defines an absolute scale for the mass of the Majorana neutrino (for reviews see, e.g., [6]). The two-neutrino double beta decay matrix element $M^{2\nu}$ is given by a sum of the GT strengths from the ground state of the initial nucleus (in our example ^{76}Ge) to all the intermediate 1^+ states in the intermediate nucleus (^{76}As) times the GT strengths from those intermediate states to the ground state of the final nucleus (^{76}Se) and divided by the corresponding energy denominator. However, a test of the two-neutrino double beta-decay calculations using the GT strengths extracted from the measured electron capture (EC) and the single-

*Electronic address: amos@physics.unimelb.edu.au

[†]Electronic address: amand.faessler@uni-tuebingen.de

[‡]Electronic address: vadim.rodin@uni-tuebingen.de

beta decay of the intermediate nucleus is only possible if the ground state in the intermediate nucleus is a 1^+ state (not the case for ^{76}As), and if the two-neutrino double beta decay is dominated by the transition through this state.

Complementary to the direct measurement of the GT strength by the EC in the first leg followed by a β^- transition from the lowest 1^+ state of the intermediate nucleus, are single-charge transfer reactions like (p, n) and $(^3\text{He}, t)$ on the ground state of the initial nucleus and (n, p) and $(d, ^2\text{He})$ to the ground state of the final nucleus; all connecting by the intermediate 1^+ states. If the forward cross section of these charge-exchange reactions are proportional to the corresponding GT strength, the two-neutrino double beta-decay probability calculations can be checked although the information about the relative phases of different contribution to can not be extracted from the experimental $B(GT)$. Then it is possible to test the quality of the calculations for the neutrinoless double beta decay.

The proportionality between the forward single charge-exchange cross section and the GT transition probabilities has been studied extensively in the past. Refs. [7] and [4] are particular contributions, with Taddeucci et al. [7] presenting a very interesting analytic study of the proportionality involving the single charge-exchange reaction (p, n) cross section at zero momentum transfer. They assumed that only angular momentum transfer $L = 0$ is important at forward scattering angles and that the eikonal approximation is valid to describe the relative motion wave functions of the incoming and emergent nucleons. Under those assumptions, they obtained an expression for the proportionality between the forward charge-exchange reaction cross section and the GT transition probability, both to 1^+ states. However, in that study [7] there are a number of other assumptions, many of which are questionable. First, a single particle-hole configura-

tion is assumed for the structure of the nuclear transitions. They also assume that the reaction mechanism can be taken in either a plane or a distorted wave impulse approximation. Furthermore, the radial wave functions for the initial neutron and for the final proton in the (p, n) reaction are assumed identical and the effects of antisymmetrization between the projectile and the target nucleon is treated rather crudely. Limiting themselves to use the impulse approximation means that they use NN amplitudes in calculations and not a specific finite ranged NN interaction. They use expressions derived by Love and Franey [8] based on Brueckner reaction matrix elements on-shell.

Ejiri [1, 2] has also made extensive study of the proportionality link. In his review [1], the proportionality of the forward charge-exchange cross section for (p, n) and $(^3\text{He}, t)$ are shown in Figs. 10 and 15 for Fermi and GT transitions, respectively. The proportionality of the charge-exchange reaction cross section to the GT strength corresponding to a (n, p) reaction is depicted in that review by using $(d, ^2\text{He})$ in Fig. 12, by using $(t, ^3\text{He})$ in Fig. 17 and by using $(^7\text{Li}, ^7\text{Be})$ in Fig. 18. Ejiri found that the proportionality of the forward scattering cross sections of single charge-exchange reactions with type (p, n) to the GT strength was good for all nuclei to mass $A = 124$. However, proportionality studies for the charge-exchange reaction of the type (n, p) was investigated only for masses to $A = 12$. Nuclei relevant for the double beta-decay proportionality of those charge-exchange reactions to the GT strengths were not considered. Such are needed of course as they are important for the two-neutrino double beta decay in the second leg where a proton changes into a neutron. Often that change cannot be effected by the GT operator $\tau^\pm \sigma$ which can only change particle types in orbits having the same quantum numbers or into the spin-orbit partner of that level.

We consider the proportionality question

again but make use of the best available reaction codes to evaluate cross sections for the charge-exchange (p, n) and (n, p) reactions. We consider specifically the very popular double beta-decay transitions $^{76}\text{Ge} \rightarrow ^{76}\text{As} \rightarrow ^{76}\text{Se}$. The nuclear structure of the initial, the intermediate and the final states in these nuclei have been defined using the Quasiparticle Random Phase Approximation (QRPA) with realistic forces (Bonn CD potential [9]) and with matrix elements calculated by solving the Bethe-Goldstone equation [10, 11]. The results show that the forward charge-exchange cross section of the type (p, n) for the first leg of the double beta decay is nicely proportional to the GT strength but that the forward reaction cross section of type (n, p) shows rather large deviations from this proportionality. The latter is due to Pauli blocking since a proton from an occupied level has to be transformed into a neutron in an empty level with the same (n, ℓ) quantum numbers. Due to the radial dependence of the NN interaction, the charge-exchange reaction can proceed by transition between SP orbits that differ in (n, ℓ) . Such effects violate the proportionality between the forward charge-exchange $((n, p) (d, ^2\text{He}), (t, ^3\text{He}), (^7\text{Li}, ^7\text{Be}) \dots)$ reaction cross sections and the GT strength.

The QRPA model of the nuclear wave functions is considered in the next Section while that of charge-exchange reaction theory is developed in Sect. III. Then, in Sect. IV we present the results and give conclusions in Sect. V

II. NUCLEAR WAVE FUNCTIONS

The majority of calculations of the two-neutrino and the neutrinoless double beta decay have been made using the QRPA [10, 11, 12, 13]. Although the starting points of all these studies are very similar, matrix elements calculated for the neutrinoless double beta-decay transition probabilities differ. For example, those obtained in

Refs. [10, 11, 12] are quite different from the ones of Ref. [13]. This is a reason to seek tests of wave functions by deriving the two-neutrino double beta-decay probability from the GT strengths between the initial and final nucleus to a large number of 1^+ states in the intermediate nucleus.

Herein we use wave functions obtained from QRPA calculations [10, 11] in which the Brueckner reaction matrix elements of the best Bonn CD potential [9] for the NN interaction are used. The strength of the NN matrix elements in the particle-particle channel is slightly adjusted, by a factor g_{pp} , to reproduce the experimental two-neutrino double beta-decay probability. For ^{76}Ge , this value is $g_{pp} = 0.85$ for a 9 level basis (pf and sdg major shells). We use the unquenched values $g_{ph} = 1$ and $g_A = 1.25$ for the particle-hole channel renormalization factor and the axial coupling constant g_A , respectively.

Any SP operator of the β^- -type can be represented in the second quantization as

$$\begin{aligned} \beta_{JM}^- &= \sum_{pn, m_p m_n} \langle pm_p | b_{JM} | nm_n \rangle a_p^\dagger a_n \\ &= \hat{J}^{-1} \sum_{pn} \langle p | | b_J | | n \rangle C^\dagger(pn, JM). \end{aligned} \quad (1)$$

In this we use $\hat{J} = \sqrt{2J+1}$, $C^\dagger(pn, JM) = [a_p^\dagger \otimes \tilde{a}_n]^{JM}$, and b_{JM} can be τ^- (Fermi), $\sigma\tau^-$ (GT), or any other operator, including ones that have r -dependence. The time reversed creation operator is defined as $\tilde{a}_{jm}^\dagger = (-)^{j-m} a_{j-m}^\dagger$. Edmond's version of the Wigner-Eckart theorem has been used.

The reduced matrix element of such SP operators between the ground state of a mother nucleus and an excited state of the daughter nucleus is given by

$$\begin{aligned} \langle J^\pi | | \beta_J^- | | 0^+ \rangle &= \hat{J}^{-1} \sum_{pn} \langle p | | b_J | | n \rangle \varrho^{(-)}(pn, J), \end{aligned} \quad (2)$$

where the elements of the transition matrices $\varrho^{(-)}(pn, J)$ are the reduced matrix elements,

$$\varrho^{(-)}(pn, J) = \langle J^\pi | | C^\dagger(pn, J) | | 0^+ \rangle. \quad (3)$$

The corresponding formulae for the β^+ -channel are obtained by the changes

$$\begin{aligned} C^\dagger(pn, J) &\rightarrow C(pn, J) \\ \varrho^{(-)}(pn, J) &\rightarrow \varrho^{(+)}(pn, J). \end{aligned} \quad (4)$$

In the RPA, an excited nuclear state having angular momentum J and projection M , is created by applying the phonon operator Q_{JM}^\dagger to the vacuum state $|0_{RPA}^+\rangle$ of the initial, even-even, nucleus:

$$|JM\rangle = Q_{JM}^\dagger |0_{RPA}^+\rangle; \quad Q_{JM} |0_{RPA}^+\rangle = 0. \quad (5)$$

Introducing the quasiparticle creation and annihilation operators, $\alpha_{\tau m_\tau}^+$ and $\alpha_{\tau m_\tau}$, ($\tau = p, n$) defined by the Bogolyubov transformation,

$$\begin{pmatrix} \alpha_{\tau m_\tau}^+ \\ \tilde{\alpha}_{\tau m_\tau} \end{pmatrix} = \begin{pmatrix} u_\tau & v_\tau \\ -v_\tau & u_\tau \end{pmatrix} \begin{pmatrix} a_{\tau m_\tau}^+ \\ \tilde{a}_{\tau m_\tau} \end{pmatrix}, \quad (6)$$

the phonon operator Q_{JM}^\dagger can be written within the QRPA as

$$Q_{JM}^\dagger = \sum_{pn} \left[X_{pn}^{(J)} A^\dagger(pn, JM) - Y_{pn}^{(J)} \tilde{A}(pn, JM) \right], \quad (7)$$

where

$$A^\dagger(pn, JM) = [\alpha_p^\dagger \otimes \alpha_n^\dagger]^{JM}, \quad (8)$$

and the forward- and backward-going free variational amplitudes X and Y satisfy the matrix equation,

$$\begin{pmatrix} \mathcal{A} & \mathcal{B} \\ \mathcal{B} & \mathcal{A} \end{pmatrix} \begin{pmatrix} X^m \\ Y^m \end{pmatrix} = \mathcal{E}_m \begin{pmatrix} 1 & 0 \\ 0 & -1 \end{pmatrix} \begin{pmatrix} X^m \\ Y^m \end{pmatrix}. \quad (9)$$

Here m identifies different roots of the QRPA equations for a given J^π and

$$\begin{aligned} \mathcal{A} &= \langle 0_{RPA}^+ | [A, [H, A^\dagger]] | 0_{RPA}^+ \rangle, \\ \mathcal{B} &= -\langle 0_{RPA}^+ | [A, [H, \tilde{A}]] | 0_{RPA}^+ \rangle. \end{aligned} \quad (10)$$

For a realistic residual interaction, the matrices \mathcal{A} and \mathcal{B} are

$$\begin{aligned} \mathcal{A}_{pn, p'n'}^{J^\pi} &= (E_p + E_n) \delta_{pp'} \delta_{nn'} \\ &\quad - \left[g_{pp} G(pn, p'n'; J) \right. \\ &\quad \times (u_p u_n u_{p'} u_{n'} + u_p u_n u_{p'} u_{n'}) \\ &\quad - g_{ph} F(pn, p'n'; J) \\ &\quad \times (u_p v_n u_{p'} v_{n'} + v_p u_n v_{p'} u_{n'}) \Big], \\ \mathcal{B}_{pn, p'n'}^{J^\pi} &= \left[g_{pp} G(pn, p'n'; J) \right. \\ &\quad \times (u_p u_n v_{p'} v_{n'} + v_p v_n u_{p'} u_{n'}) \\ &\quad - g_{ph} F(pn, p'n'; J) \\ &\quad \times (u_p v_n v_{p'} u_{n'} + v_p u_n u_{p'} v_{n'}) \Big], \end{aligned}$$

where $G(pn, p'n', J)$ and $F(pn, p'n', J)$ are particle-particle and particle-hole interaction matrix elements of a G-matrix, respectively.

Within the QRPA, one has

$$\begin{aligned} C^\dagger(pn, JM) &= u_p v_n A^\dagger(pn, JM) \\ &\quad + v_p u_n \tilde{A}(pn, JM), \end{aligned} \quad (11)$$

and the transition matrix takes the form,

$$\begin{aligned} \varrho^{(-)}(pn, J) &= \hat{J}(u_p v_n X_{pn}^{(J)} + v_p u_n Y_{pn}^{(J)}), \\ \varrho^{(+)}(pn, J) &= \hat{J}(v_p u_n X_{pn}^{(J)} + u_p v_n Y_{pn}^{(J)}). \end{aligned} \quad (12)$$

Correspondingly, the $B(GT)$ values for the GT transitions $0^+ \rightarrow 1^+$ can be written as

$$\begin{aligned} B(GT^{(-)}) &= |\langle 1^+ | \sum_a \sigma_a \tau_a^- | 0^+ \rangle|^2 \\ &= \left| \sum_{pn} \langle p | \sigma | n \rangle \right. \\ &\quad \times (u_p v_n X_{pn}^{(1+)} + v_p u_n Y_{pn}^{(1+)})) \Big|^2, \\ B(GT^{(+)}) &= |\langle 1^+ | \sum_a \sigma_a \tau_a^+ | 0^+ \rangle|^2 \\ &= \left| \sum_{pn} \langle n | \sigma | p \rangle \right. \\ &\quad \times (v_p u_n X_{pn}^{(1+)} + u_p v_n Y_{pn}^{(1+)})) \Big|^2. \end{aligned} \quad (13)$$

In calculations, a harmonic oscillator with an oscillator length parameter $b = 2.09$ fm is used to specify the SP wave functions for ^{76}Ge and ^{76}Se . Those functions are positive at the origin. Using $N=3$ and $N=4$ oscillations

TABLE I: Two-quasiparticle configurations forming the QRPA structure of 1^+ states in ^{76}As (relative to the ground state in ^{76}Se) and corresponding without pairing to particle-hole states.

ID	q-p	q-h	ID	q-p	q-h
	$n\ell j$	$n\ell j$		$n\ell j$	$n\ell j$
1	$0f_{7/2}$	$0f_{7/2}$	13	$0g_{7/2}$	$0g_{9/2}$
2	$0f_{7/2}$	$0f_{5/2}$	14	$0g_{7/2}$	$0g_{7/2}$
3	$0f_{5/2}$	$0f_{7/2}$	15	$0g_{7/2}$	$1d_{5/2}$
4	$0f_{5/2}$	$0f_{5/2}$	16	$1d_{5/2}$	$0g_{7/2}$
5	$0f_{5/2}$	$1p_{3/2}$	17	$1d_{5/2}$	$1d_{5/2}$
6	$1p_{3/2}$	$0f_{5/2}$	18	$1d_{5/2}$	$1d_{3/2}$
7	$1p_{3/2}$	$1p_{3/2}$	19	$1d_{3/2}$	$1d_{5/2}$
8	$1p_{3/2}$	$1p_{1/2}$	20	$1d_{3/2}$	$1d_{3/2}$
9	$1p_{1/2}$	$1p_{3/2}$	21	$1d_{3/2}$	$2s_{1/2}$
10	$1p_{1/2}$	$1p_{1/2}$	22	$2s_{1/2}$	$1d_{3/2}$
11	$0g_{9/2}$	$0g_{9/2}$	23	$2s_{1/2}$	$2s_{1/2}$
12	$0g_{9/2}$	$0g_{7/2}$			

tor shells in the QRPA calculations for transitions to 1^+ states in ^{76}As gives a set of 23 two-quasiparticle excitations per Eq. (8) to be included, via Eqs. (7) and (5), into the QRPA phonon creation operator for 1^+ states in ^{76}As [10, 11]. That set is shown in Table I. The individual components are identified by the label ID which will be used in the discussion of results. Of those two-quasiparticle states, the ones labelled with ID = 5, 6, 15, 16, 21 and 22 cannot be excited by the Gamow-Teller (GT) operator.

In Fig. 1, a set of one-body density matrix elements, $\rho^{(\pm)}$ of Eq. (3) (OBDME hereafter), for the excitation of five particular 1^+ states of the 23 found with this model structure are shown with for each of the 23 components (ID). They are states of special interest regarding the $^{76}\text{Se}(n, p)$ zero-degree cross

sections considered later; being the strongest of the 23 charge-exchange excitations considered. Of note is that the strongest OBDME $\rho^{(+)}$ of the fourth state belongs to the two-quasiparticle state $1p_{3/2}-0f_{5/2}$ (ID=5). That component, readily excited in the charge-exchange reaction, cannot be excited by the GT operator. Thus, one may anticipate that the proportionality between the charge-exchange reaction cross section and the GT strength for this state may be different to those of others.

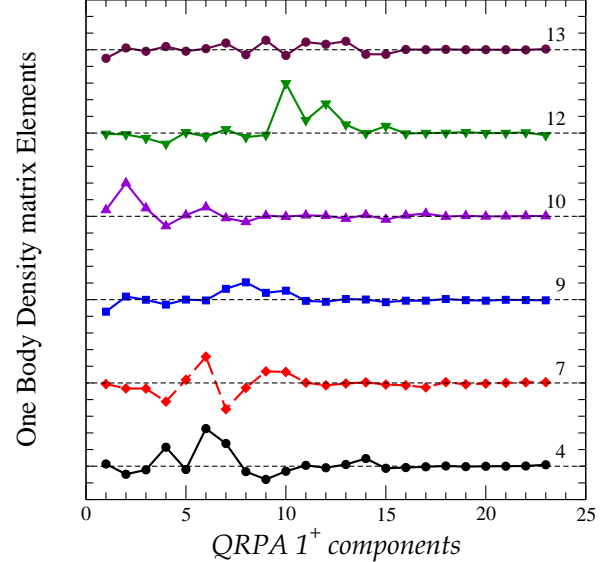


FIG. 1: One-body density matrix elements $\rho^{(+)}(pn, 1^+)$ of Eq. (12), in arbitrary units, as a function of the two-quasiparticle components labeled according to Table I.

III. REACTION THEORY

The charge-exchange reaction is described in a distorted wave approximation (DWA) in which one requires transition structure details, optical model wave functions (the distorted waves), and a transition operator by which the reaction is effected.

Consider first the distorted wave functions. Conventionally these are the relative motion wave functions ascertained from an optical potential from which good fits to elastic scattering data (cross sections and spin observables) has been obtained. In many studies those potentials have been assumed to be local in form and usually of Woods-Saxon type with parameters adjusted to find a good fit to elastic scattering data. But the associated relative motion wave functions are not guaranteed to be proper. Only the asymptotic (large radius) properties are tested by such data fitting.

A more physical approach is to form optical potentials by folding a NN interaction with the target ground state structure. In that way one can also ensure that the Pauli principle is not violated. However, once the target structure has been set, then one has to choose the NN interaction. For some time now it has been known that the interaction differs from the free NN one. Medium effects lead to the effective NN interaction being energy- and density-dependent as well as complex. The current best practice, at least for energies below 3-3 resonance excitation, is to use an effective interaction built from the NN g -matrices that are solutions of the Bethe-Brueckner-Goldstone (BBG) equations [14]. Using those g -matrices, both on- and off-shell values and for 32 NN angular momentum channels, lead to an effective NN interaction in coordinate space that is a mixture of central, two-nucleon spin-orbit, and two-nucleon tensor components. Details of that mapping are given elsewhere [14].

Of great importance is that on using such an effective NN interaction in forming optical potentials, and when account is taken of the Pauli principle, those optical potentials are strongly non-local and partial wave dependent. The non-locality arises from the allowance for knock-out (exchange) amplitudes in the so-called g -folding procedure [14]. Doing so requires more than just the densities of the nuclear ground state. One requires the

ground state OBDME

$$\rho_{gs} = \langle 0_{gs}^+ | [a_j^\dagger \otimes \tilde{a}_j]^{(J=0)} | 0_{gs}^+ \rangle. \quad (14)$$

Assuredly, the relative motion wave functions will differ from those found using phenomenological (local) potentials even if the potentials are phase equivalent. The Perey effect is one ramification. Exchange effects are also most important in evaluations of non-elastic scattering and that will be discussed later.

In coordinate space, the g -folding optical potential can be written

$$\begin{aligned} U(\mathbf{r}, \mathbf{r}'; E) &= \delta(\mathbf{r} - \mathbf{r}') \int \rho(\mathbf{s}) g^D(\mathbf{r}, \mathbf{s}; E) d\mathbf{s} \\ &\quad + \sum_i n_i \varphi_i^*(\mathbf{r}) g^{Ex}(\mathbf{r}, \mathbf{r}'; E) \varphi_i(\mathbf{r}'); \\ \rho(\mathbf{s}) &= \sum_i n_i \varphi_i^*(\mathbf{s}) \varphi_i(\mathbf{s}). \end{aligned} \quad (15)$$

Here $\rho(\mathbf{s})$ is the nucleon density for nucleons with the occupancies n_i . To evaluate these potentials requires specification of three quantities. They are the single nucleon bound state wave functions $\varphi_i(\mathbf{r})$, the orbit occupancies n_i , which more properly are the nuclear OBDME of Eq. (14), and the NN g -matrices $g^{D/Ex}(\mathbf{r}, \mathbf{s}; E)$. Those g -matrices are appropriate combinations of NN interactions in the nuclear medium for diverse NN angular momentum channels [14]. For the latter, much success has been had using an effective NN interaction, now commonly designated as the Melbourne force [14], and which has the form $g_{01}^{ST} \equiv g_{eff}^{ST}(\mathbf{r}, E; k_f(R))$ where $\mathbf{r} = \mathbf{r}_0 - \mathbf{r}_1$ and $R = \frac{1}{2}|(\mathbf{r}_0 + \mathbf{r}_1)|$. It is based on the g -matrix of the Bonn B potential [15]. In the prescription, the Fermi momenta relate to the local density in the nucleus at distance R from the center when \mathbf{r}_i are the coordinates of the colliding projectile and bound nucleons. $\{ST\}$ are the spin and isospin quantum numbers of the NN system.

For use in the DWBA98 program [16], these effective NN g -matrices are, specifi-

cally,

$$\begin{aligned}
g_{eff}^{ST} &= g_{eff}^{ST}(\mathbf{r}, E; k_f) \\
&= \sum_{i=1}^3 \left[\sum_{j=1}^4 S_j^{(i)}(E; k_f) \frac{e^{-\mu_j^{(i)} r}}{r} \right]_{[S,T]} \Theta_i \\
&= \sum_{i=1}^3 g_{eff}^{(i)ST}(r, E; k_f) \Theta_i,
\end{aligned} \tag{16}$$

where Θ_i are the characteristic operators for central forces ($i = 1$), $\{1, (\sigma \cdot \sigma), (\tau \cdot \tau), (\sigma \cdot \sigma \tau \cdot \tau)\}$, for the tensor force ($i = 2$), $\{\mathbf{S}_{12}\}$, and for the two-body spin-orbit force ($i = 3$), $\{\mathbf{L} \cdot \mathbf{S}\}$. The $S_j^{(i)}(E; k_f)$ are complex, energy- and density-dependent strengths. The properties of the g -matrices are such that, not only can the ranges of the Yukawa form factors be taken as independent of energy and density [14], but also four suffice for energies in the range 25 to 300 MeV.

The strengths (and ranges) in these effective NN interactions were found by mapping their double Bessel transforms to the NN g -matrices in infinite nuclear matter (solutions of the BBG equations). With α : $\{LL'JST\}$, this mapping is

$$g_{eff;LL'}^{JST}(q', q; E) = \sum_i \langle \Theta_i \rangle \mathcal{I}_i, \tag{17}$$

where the radial integrals expand to

$$\begin{aligned}
\mathcal{I}_i &= \int_0^\infty r^{2+\lambda} j_L(q'r) g_{eff}^{(i)ST}(r, E; k_f) j_{L'}(qr) dr \\
&= \sum_j S_j^{(i)}(\omega) \\
&\quad \times \int_0^\infty r^{2+\lambda} j_L(q'r) \frac{e^{-\mu_j^{(i)} r}}{r} j_{L'}(qr) dr \\
&= \sum_j S_j^{(i)}(\omega) \tau^\alpha(q', q; \mu_j^{(i)}).
\end{aligned} \tag{18}$$

Therein $\lambda = 2$ for the tensor force. In application, a singular valued decomposition has been used to effect this mapping.

With the distorted wave approximation (DWA) for inelastic scattering amplitudes,

the g -folding model has been used to determine the distorted waves in both the incident and emergent channels. In addition, the same effective NN interaction [14] has been used as the transition operator. A microscopic model of structure is needed to give the transition OBDME required. The single nucleon wave functions used to form the optical potentials also are used for the single nucleon states in each term in the inelastic scattering amplitude.

In the DWA, amplitudes for an inelastic scattering through a scattering angle of θ and between the states $|J_i, M_i\rangle$ and $|J_f, M_f\rangle$ in a nucleus, are

$$\begin{aligned}
T_{DWA} &= T_{J_f J_i}^{M_f M_i \nu' \nu}(\theta) \\
&= \left\langle \chi_{\nu'}^{(-)}(\mathbf{k}_0 0) \right| \left\langle \Psi_{J_f M_f}(1 \cdots A) \right| \\
&\quad \times A \sum_{ST} g_{eff}^{ST}(\mathbf{r}_{0,1}, E; k_f) P_S P_T \\
&\quad \times \mathcal{A}_{01} \left\{ \left| \chi_{\nu}^{(+)}(\mathbf{k}_i 0) \right\rangle \right| \Psi_{J_i M_i}(1 \cdots A) \rangle \},
\end{aligned} \tag{19}$$

where ν, ν' are the spin quantum number of the nucleon in the continuum, $\chi^{(\pm)}$ are the distorted waves, and $g_{eff}^{ST}(\mathbf{r}_{0,1}, E; k_f) P_S P_T$ is the spin-isospin Melbourne force. The operator \mathcal{A}_{01} effects the antisymmetrization of the two-nucleon product states.

Then, by using cofactor expansions, $|\Psi_{JM}\rangle = A^{-1/2} \sum_{j,m} |\varphi_{jm}(1)\rangle a_{jm} |\Psi_{JM}\rangle$, the matrix elements become

$$\begin{aligned}
T_{J_f J_i}^{M_f M_i \nu' \nu} &= \sum_{j_1, j_2 i, S, T} \langle \Psi_{J_f M_f} | a_{j_2 m_2}^\dagger a_{j_1 m_1} | \Psi_{J_i M_i} \rangle \\
&\times \left\langle \chi_{\nu'}^{(-)}(\mathbf{k}_0 0) \right| \left\langle \varphi_{j_2 m_2}(1) \right| g_{eff}^{ST}(\mathbf{r}_{0,1}, E; k_f) \\
&\quad \times P_S P_T \mathcal{A}_{01} \left\{ \left| \chi_{\nu}^{(+)}(\mathbf{k}_i 0) \right\rangle \right| \varphi_{j_1 m_1}(1) \rangle \}.
\end{aligned} \tag{20}$$

The density matrix elements in the ampli-

tudes reduce as

$$\begin{aligned}
& \left\langle \Psi_{J_f M_f} \left| a_{j_2 m_2}^\dagger a_{j_1 m_1} \right| \Psi_{J_i M_i} \right\rangle \\
&= \sum_{I(N)} (-1)^{(j_1 - m_1)} \langle j_1, j_2, m_1, -m_2 | I, N \rangle \\
&\quad \times \left\langle \Psi_{J_f M_f} \left| \left[a_{j_2}^\dagger \otimes a_{j_1} \right]^{IN} \right| \Psi_{J_i M_i} \right\rangle \\
&= \sum_{I(N)} (-1)^{(j_1 - m_1)} \langle j_1, j_2, m_1, -m_2 | I, N \rangle \\
&\quad \times \langle J_i, I, M_i, N | J_f, M_f \rangle \frac{1}{\sqrt{2J_f + 1}} S_{j_1 j_2 I}, \tag{21}
\end{aligned}$$

where $S_{j_1 j_2 I}$ are the transition OBDME. The DWA amplitudes are then

$$\begin{aligned}
T_{J_f J_i}^{M_f M_i \nu' \nu} &= \sum_{\xi} \frac{(-1)^{(j_1 - m_1)}}{\sqrt{2J_f + 1}} S_{j_1 j_2 I} \\
&\times \langle j_1, j_2, m_1, -m_2 | I, N \rangle \langle J_i, I, M_i, N | J_f, M_f \rangle \\
&\times \left\langle \chi_{\nu'}^{(-)}(\mathbf{k}_0 0) \right| \langle \varphi_{j_2 m_2}(1) | \mathbf{g}_{eff}^{ST}(\mathbf{r}_{0,1}, E; k_f) \right. \\
&\quad \left. \times P_S P_T \mathcal{A}_{01} \left\{ \left| \chi_{\nu}^{(+)}(\mathbf{k}_i 0) \right\rangle \right| \varphi_{j_1 m_1}(1) \right\rangle. \tag{22}
\end{aligned}$$

In this, $\{\xi\} = j_1, j_2, m_1, m_2, I(N), S, T$ with j_2 being the particle and j_1 the hole in a particle-hole specification of the transition.

Thus, in our DWA evaluations of the charge-exchange scattering of interest, namely $^{76}\text{Ge}(p, n)$ and $^{76}\text{Se}(n, p)$ to 1^+ states given by a QRPA model, we have used

1. SP wave functions: harmonic oscillators with oscillator length of 2.09 fm. Those are used to specify both the optical potentials and the reaction amplitudes.
2. Optical potentials (to give the distorted waves) are formed with the Melbourne effective NN interaction at the relevant incident particle energies. The occupancies of the single particle level are automatically given in the QRPA

due to pairing and configuration mixing and are contained in the OBDME in Eq. (12).

3. The same effective interactions are used in evaluations of the charge-exchange cross sections.
4. The $\rho^{(\pm)}$ of Eq. (12) are taken as the $S_{j_1 j_2, I=1}$ depending upon which reaction, (p, n) or (n, p) , is described.

IV. RESULTS

Differential cross sections evaluated at zero degree scattering and the total reaction cross sections from $^{76}\text{Ge}(p, n)$ and $^{76}\text{Se}(n, p)$ leading to the first 1^+ state in ^{76}As are displayed in Fig. 2. The results found at energies of 40, 65, 100, and 200 MeV, are connected by solid lines (0° cross sections) and by dashed lines (reaction cross sections). The results of $^{76}\text{Ge}(p, n)$ to the first excited 1^+ state in ^{76}As are larger than those of $^{76}\text{Se}(n, p)$ to the same first excited 1^+ state. Over these energies, those ratios range from 25 to 65. It is intriguing that both the zero-degree differential cross sections, which increase monotonically over these energies, and the reaction cross sections, which decrease accordingly, have such similar ratios.

The scale factors are not simply a zero-degree phenomenon. This is emphasized by the differential cross-section results for the four energies displayed in Fig. 3 to $\theta_{cm} = 10^\circ$. The results in the top of this figure for the four energies as indicated, are those from the charge-exchange (p, n) reaction. The other (smaller in magnitude) results are the differential cross sections for the (n, p) reaction. The reduction is an effect of the Pauli principle. In $^{76}\text{Ge}_{44}$, the proton Fermi surface lies between the $1p_{3/2}$ and the $0f_{5/2}$ levels while the neutron Fermi surface lies within the $0g_{9/2}$ single-particle state. For the (p, n)

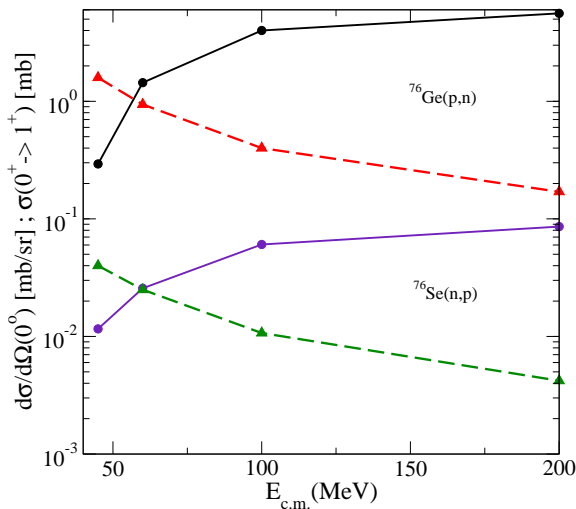


FIG. 2: Zero-degree differential cross sections (filled circles) and total reaction cross sections (filled triangles) from $^{76}\text{Ge}(p,n)$ and $^{76}\text{Se}(n,p)$ to the first excited 1^+ state in ^{76}As .

charge-exchange reaction, one must move a neutron into a proton level. In these nuclei the GT transition operator $\tau^-\sigma$ can make a nucleon into a single particle level with the same quantum numbers or to the spin-orbit partner. This is possible for transitions $0f_{5/2} \rightarrow 0f_{5/2}$, $1p_{1/2} \rightarrow 1p_{1/2}$ and $0g_{9/2} \rightarrow 0g_{9/2}$. But for the inverse reaction, (n,p) on $^{76}\text{Se}_{42}$, all the possible single-particle GT transitions are strongly Pauli hindered, if not Pauli blocked. The latter cases allow GT transitions since the GT operator can only move a proton into a corresponding neutron level of the same $(n\ell j)$ orbit or the spin-orbit partner because of the smearing of the Fermi surface which is mainly induced by pairing correlations. For the charge-exchange reaction (n,p) on the other hand, the finite range character of the transition operator and the knock-out process associated with antisymmetrization allow non-GT type transitions to contribute.

The foregoing has dealt only with the excitation of the first 1^+ state in ^{76}As . We now

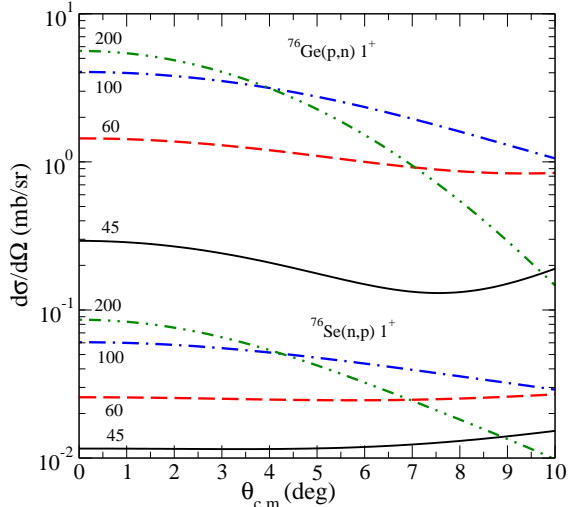


FIG. 3: Differential cross sections from the two charge-exchange reactions leading to the first 1^+ state in ^{76}As for bombarding energies of 45 (solid curves), 60 (dashed curves), 100 (dashed-dotted curves) and 200 (double dot-dashed curves) MeV.

consider the zero-degree cross sections for all 23 possible QRPA defined 1^+ states and their ratios to the corresponding GT strengths. In Table II those cross-section values calculated for the $^{76}\text{Ge}(p,n)$ and $^{76}\text{Se}(n,p)$ reactions to each of the 23 excited 1^+ states obtained by QRPA in ^{76}As are listed in columns 2 and 4. The ratios of those with the corresponding GT strengths are listed in columns 3 and 5.

State 16 corresponds to the GT resonance that is reflected by the large (p,n) cross section at zero degree scattering being 51 mb/sr. The corresponding GT strength has a dimensionless value of 12.8. The states 7, 9, 11, 15 and 16 have differential (p,n) cross sections at zero-degree scattering larger than 10 mb/sr. The ratio to the GT strength for these five states are 4.16, 3.96, 3.47, 4.05 and 4.02. The ratio for these five leading states therefore lies between 3.47 and 4.16; and so there is about 20% variation relative to the

TABLE II: Differential cross sections at zero degrees scattering for the charge-exchange reactions $^{76}\text{Ge}(p, n)$ and $^{76}\text{Se}(n, p)$ exciting $^{76}\text{As}(1^+, m)$. The projectile energy in all cases was 200 MeV. \mathcal{R} are the ratios of each of those cross sections with the associated, dimensionless, GT strength.

m	$^{76}\text{Ge}(p, n)(0^\circ)$	\mathcal{R}	$^{76}\text{Se}(n, p)(0^\circ)$	\mathcal{R}
1	5.61	3.73	0.09	3.15
2	1.74	5.55	1×10^{-3}	25.48
3	1.01	5.27	0.03	10.96
4	2.35	6.19	0.22	6.93
5	1.07	3.80	3×10^{-4}	571.43
6	3.04	4.95	3×10^{-3}	40.12
7	12.28	4.16	0.26	3.71
8	2.31	3.56	0.08	3.54
9	15.01	3.96	0.38	3.10
10	0.34	5.45	0.18	6.27
11	18.43	3.47	0.04	3.40
12	4.77	4.09	0.31	3.83
13	3.98	4.21	0.24	4.29
14	9.40	4.01	0.01	4.77
15	10.05	4.05	0.05	3.63
16	51.52	4.02	0.01	3.91
17	1.49	3.93	3×10^{-4}	8.93
18	0.08	3.94	2×10^{-3}	4.25
19	0.14	4.14	0.01	4.16
20	0.27	3.98	0.02	3.92
21	5×10^{-3}	4.10	2×10^{-5}	3.20
22	0.02	4.87	7×10^{-4}	6.13
23	0.10	4.21	0.02	4.58

mean value. The six largest values for the $^{76}\text{Se}(n, p)$ cross section at zero degree scattering are obtained for the states identified as 4, 7, 9, 10, 12 and 13 in the sequence. The ratios of these cross sections to their corresponding GT strengths vary between 3.1 and 6.9. Thus for these six largest (n, p) transitions, there is a variation in the ratio of the zero-degree charge-exchange cross section to the GT strength of about 80%. This is large

in comparison to the variation in the ratios involving the strongest (p, n) reaction cross sections.

In Fig. 4 the zero-degree cross sections for $^{76}\text{Ge}(p, n)^{76}\text{As}(1^+, m)$; $m = 1, \dots, 23$ are shown by the filled circles that are connected by dashed lines. The filled squares connected by the solid lines are the dimensionless GT strengths of the operator of Eq. (13), $B(GT^{(-)}, {}^{76}\text{Ge} \rightarrow {}^{76}\text{As})$, for transition to each state of the QRPA given in sequence in Table II. The charge-exchange cross section values, connected by the dashed lines, resulted from DWA calculations made using the full NN interaction (Melbourne force) as the transition operator. The open circles are results obtained when only the central part of that transition operator was used. Clearly, for zero-degree scattering, the two-body spin-orbit and tensor contributions do not effect the cross sections appreciably. The proton incident energy for all (p, n) reactions is 200 MeV.

Clearly the zero-degree cross sections for all (p, n) transitions track similarly to the GT strengths of the same states. For the (p, n) , and presumably also for the corresponding reactions $(^3\text{He}, t)$, the proportionality between those charge-exchange reaction cross sections in the forward direction and the GT strengths is fulfilled quite well. As noted above, that means a proportionality within about 20% for the five strongest transitions.

The situation is different for the (n, p) reactions, and presumably also for the corresponding reactions $(t, {}^3\text{He})$ and $({}^7\text{Li}, {}^7\text{Be})$. That is evident both from inspection of the results in Table II and in Fig. 5. For these transitions, most components are Pauli forbidden so far as the GT operator is concerned. Finite values occur only due to a smearing of the Fermi surfaces. But the (n, p) reactions, while hindered similarly, also can proceed by excitation of other components in the wave functions.

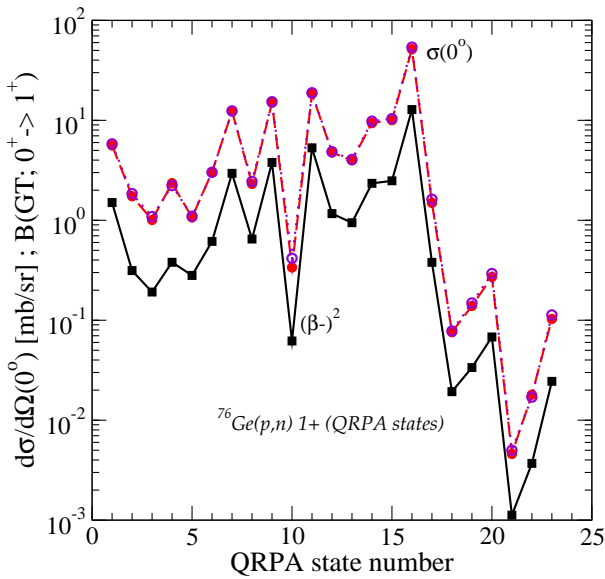


FIG. 4: Differential cross sections at zero-degree scattering from DWA calculations of $^{76}\text{Ge}(p,n)^{76}\text{As}(1^+,m)$. Results found with and without non-central components in the transition operator are depicted by the filled and open circles respectively. The filled squares are the values of $B(\text{GT}^-)$ for $^{76}\text{Ge} \rightarrow ^{76}\text{As}(1^+,m)$ for each 1^+ state.

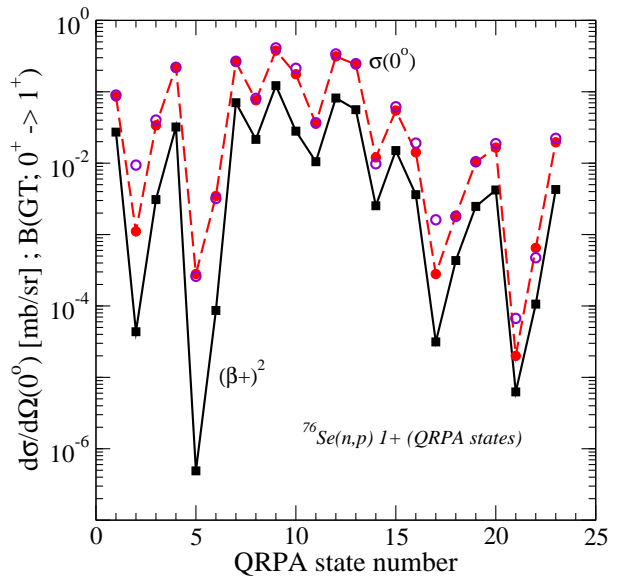


FIG. 5: Differential cross sections at zero degree scattering for $^{76}\text{Se}(n,p)$ to the 23 1^+ states in ^{76}As (filled circles connected by dashed lines). The DWA results found by restricting the transition operator to just the central terms are depicted by the open circles. The associated GT strengths are shown by the filled squares connected by solid lines.

From Fig. 5 it is evident that the (n,p) cross sections variation over the 23 QRPA possible states still tracks the values of the associated GT strengths. However, note that both cross sections and GT strengths are much smaller than their counterparts in Fig. 4, and the omission of non-central force elements in DWA calculations makes some greater variation than seen with the (p,n) results. Consequently, the proportionality ‘constant’ of the ratio of forward direction, (n,p) charge-exchange cross sections to the GT strengths for the six strongest transition is very large.

As the specifics of the Melbourne force change with incident energy, and particularly those of the non-central components, we have made DWA calculations at other energies. At 120 MeV, the zero-degree cross section val-

ues and their ratios with the associated GT strengths are listed in Table III. As with the 200 MeV results, the proportionality between the charge-exchange cross sections calculated at zero degree scattering and the GT strength is fulfilled to within about 20% for the reaction $^{76}\text{Ge}(p,n)$. However, the variation is much larger for the ratios with the cross sections for $^{76}\text{Se}(n,p)$. In fact the variation of the latter ratios is near 90% when one considers only the strongest (n,p) transitions.

In Fig. 6, the zero-degree cross sections from our DWA evaluations of all $^{76}\text{Se}(n,p)$ reactions to the QRPA 1^+ states in ^{76}As are shown for an incident neutron energy of 120 MeV. As before, those results are depicted by the filled and open circles (connected by the

TABLE III: The zero-degree charge-exchange cross sections and ratios (\mathcal{R}) of them to the associated GT strength for the $^{76}\text{Ge}(p, n)$ ^{76}As and $^{76}\text{Se}(n, p)$ ^{76}As reactions to $^{76}\text{As}(1^+, m)$. In this case, the incident energy was 120 MeV.

m	$^{76}\text{Ge}(p, n)(0^\circ)$	\mathcal{R}	$^{76}\text{Se}(n, p)(0^\circ)$	\mathcal{R}
1	6.51	4.33	0.10	3.58
2	2.40	7.64	9×10^{-3}	210.10
3	1.47	7.67	0.05	17.26
4	2.98	7.85	0.28	8.80
5	1.32	4.70	6×10^{-4}	1146.9
6	3.73	6.07	2×10^{-3}	25.56
7	14.85	5.03	0.31	4.35
8	2.77	4.26	0.09	4.13
9	17.47	4.61	0.46	3.73
10	0.46	7.45	0.24	8.68
11	21.52	4.06	0.04	3.91
12	5.65	4.84	0.37	4.56
13	4.81	5.08	0.24	4.19
14	11.07	4.73	0.02	8.06
15	11.83	4.76	0.07	4.50
16	61.63	4.81	0.02	6.29
17	1.84	4.86	2×10^{-3}	49.43
18	0.09	4.51	2×10^{-3}	5.12
19	0.17	5.06	0.01	4.68
20	0.33	4.87	0.02	4.91
21	6×10^{-3}	4.90	7×10^{-5}	10.88
22	0.02	5.68	9×10^{-4}	8.10
23	0.11	4.54	0.02	4.65

dashed lines to guide the eye), with the filled circle presenting the results when the complete Melbourne force is used and the open circles giving the results when only the central force components are considered. The associated GT strengths are depicted by the filled squares connected by the solid lines. As with the results for 200 MeV, the (n, p) cross section values vary across the 23 QRPA cases very similarly to the GT strength values. But the devil is in the differences again and the ratio of them is far removed from being con-

stant over the set.

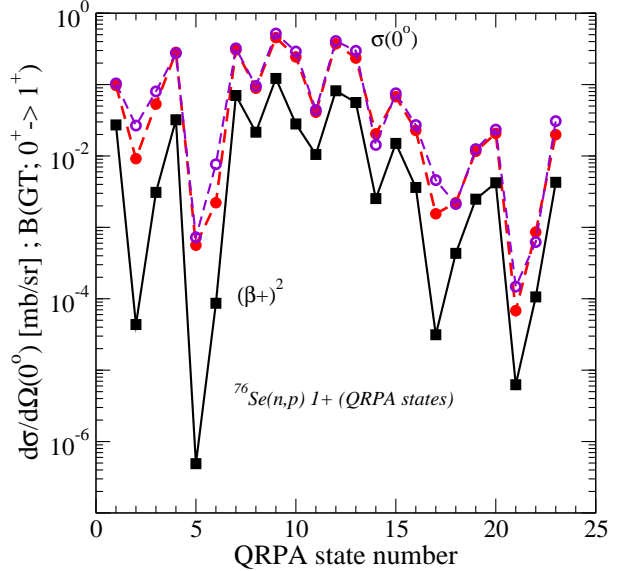


FIG. 6: Zero-degree differential cross sections from DWA calculations of 120 MeV $^{76}\text{Se}(n, p)$ to 1^+ excited states in ^{76}As and the associated GT strengths. Details are given in the text.

Finally, in Figure 7 we plot the ratios of our calculated zero-degree charge-exchange cross sections and GT strengths for the transition $^{76}\text{Ge} \rightarrow ^{76}\text{As}$ (filled circles connected by a solid lines) to the 23 QRPA states in ^{76}As for the incident proton energy of 200 MeV. The ratios for $^{76}\text{Se}(n, p)$ ^{76}As cross sections are displayed by the open diamonds connected by the dashed lines (200 MeV) and by the filled triangles connected by the dot-dashed lines (120 MeV). On this scale the relative smoothness of the ratios for all 23 QRPA cases of $^{76}\text{Ge} \rightarrow ^{76}\text{As}$ is apparent. The variation though is $\sim 20\%$. But the extreme variation over the set for the $^{76}\text{Se}(n, p)$ ^{76}As ratios makes it impossible to consider such as forming a proportionality constant. Even restricting consideration to the five strongest (n, p) transitions yields a variation of $\sim 90\%$.

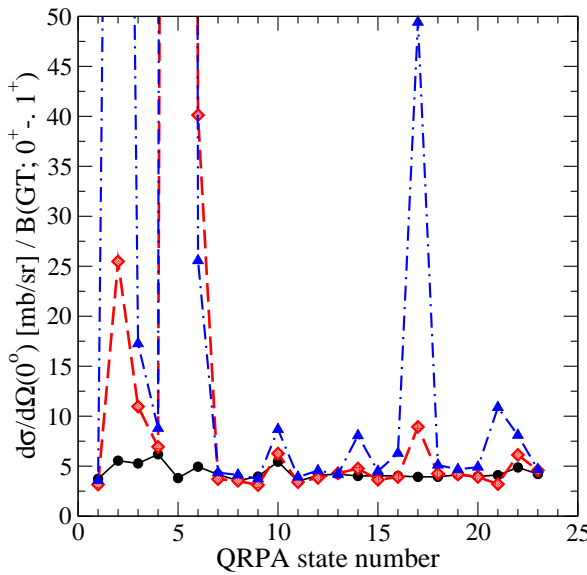


FIG. 7: Ratios of cross sections from $^{76}\text{Ge}(p,n)$ ^{76}As evaluated at zero degree scattering with the GT strengths (filled circles) for an incident energy of 200 MeV and for $^{76}\text{Se}(n,p)$ ^{76}As displayed for 200 MeV (open diamonds) and for 120 MeV (filled triangles).

V. CONCLUSIONS

In conclusion, from our analysis of excitations in medium mass nuclei, the proportionality between forward differential cross sections and GT strengths is fulfilled to within about 20% for (p,n) (and, we expect, the

same for $^3(\text{He},t)$) reactions. But this is not the case with forward differential charge-exchange (n,p) reactions, and presumably with $(d, ^2\text{He})$, $(t, ^3\text{He})$ and $(^7\text{Li} ^7\text{Be})$ reactions. In light nuclei, where protons and neutrons fill the same or nearly the same single-particle levels, the proportionality of forward charge-exchange reaction cross sections and the GT strengths seems valid for both (n,p) and (p,n) processes. For them the proton and neutron Fermi surfaces are similar. But that is not so for medium-heavy nuclei. For them the proton and neutron Fermi surfaces are quite different, so that the effects of Pauli-blocking (hindering for smeared surfaces) allows the proportionality to be good (within 20%) for (p,n) -like processes but not for (n,p) -like transitions.

Acknowledgments

We are most grateful to Prof. Herbert Müther for providing us with solutions of the Bethe-Goldstone equation starting with the Bonn-CD NN force. The work of V. R. has been supported by the Deutsche Forschungsgemeinschaft (by grant FA67/28-2 and within the Transregio Project TR27 “Neutrinos and Beyond”). A. F. and V. R. thank also the EU ILIAS project under the contract RII3-CT-2004-506222 for a support.

[1] H. Ejiri, Phys. Rep. **338**, 265 (2000).
 [2] H. Ejiri, Nucl. Phys. **A687**, 350c (2001).
 [3] S. Rakers et al., Phys. Rev. C **65**, 044323 (2002); C. Bäumer et al., *ibid.* **68**, 031303 (R) (2003).
 [4] S. Rakers et al., Phys. Rev. C **70**, 054302 (2004).
 [5] S. Rakers et al., Phys. Rev. C **71**, 054313 (2005).
 [6] A. Faessler, F. Simkovic; J. Phys. **G24** (1998) 2139; S. R. Elliott and P. Vogel, Ann. Rev. Nucl. Part. Sci. **52**, 115 (2002); R.D. McKeown, P. Vogel; Phys. Rep. **394** (2004) 315
 [7] T. N. Taddeucci et al., Nucl. Phys. **A469**, 125 (1987).
 [8] W. G. Love and M. A. Franey, Phys. Rev. C **24**, 1073 (1981).
 [9] R. Machleidt, F. Sammarruca, and Y. Song, Phys. Rev. C **53**, R1483 (1996).
 [10] V. Rodin, A. Faessler, F. Simkovic, and P. Vogel, Phys. Rev. C **69**, 044302 (2003).

- [11] V. Rodin, A. Faessler, F. Simkovic, and P. Vogel, Nucl. Phys. **A766**, 107 (2006).
- [12] K. Muto, Phys. Lett. **B391**, 343 (1997).
- [13] O. Civitarese and J. Suhonen, Nucl. Phys. **A752**, 53 (2005).
- [14] K. Amos, P. J. Dortmans, H. V. von Geramb, S. Karatagliidis, and J. Raynal, Adv. in Nucl. Phys. **25**, 275 (2000).
- [15] R. Machleidt, K. Holinde, and C. Elster, Phys. Rep. **149**, 1 (1987).
- [16] J. Raynal, *computer program dwba98, nea 1209/05* (1998).